

Microstructural Changes of High Strength Concrete during Low Cycle Compression Fatigue Test after Exposure to High Temperature

Dongfu Zhao^{1,2,3,4}, Wenbo He^{1*}, Peiyuan Hao¹

¹ School of Civil and Transportation Engineering, Beijing University of Civil Engineering and Architecture, Zhanlanguan Road 1#, Beijing 100044, China

² Beijing Energy Conservation & Sustainable Urban and Rural Development Provincial and Ministry Co-construction Collaboration Innovation Center, Beijing 100044, China

³ Multi-Functional Shaking Tables Laboratory, Beijing University of Civil Engineering and Architecture, Beijing 100044, China

⁴ Beijing Higher Institution Engineering Research Center of Civil Engineering Structure and Renewable Material, Beijing 100044, China

* Corresponding author, e-mail: 2108590020105@stu.bucea.edu.cn

Received: 11 November 2022, Accepted: 30 April 2023, Published online: 15 May 2023

Abstract

Using ultrasonic detection, microhardness test, scanning electron microscope test, mercury intrusion method and X-ray diffraction, the parameters of sonic time, microhardness, pore size distribution, cumulative pumping of high strength concrete under low cycle compression loading are tested after exposure to 200 °C, 400 °C and 600 °C. Experimental study showed that with the increasing loading times, the rangeability of sonic time, the microhardness, and total pore volume shows an overall trend of fast-slow-fast. Furthermore, the sonic time and microhardness are linearly related to the longitudinal fatigue strain. The research results provided references for nondestructive testing, fatigue damage analysis and structural evaluation of concrete structures subjected to fire or other high temperature processes.

Keywords

high strength concrete, high temperature, low cycle compression loading, microstructure

1 Introduction

High strength concrete (HSC) materials have high compressive strength and large bearing capacity, and are widely used in modern building structures such as high-rise and long-span buildings. However, when exposed to high temperatures during a fire, the dense internal structure of the material can lead to poor permeability and easy cracking, causing high-strength concrete components to quickly lose their load-bearing capacity. Furthermore, engineering structures that have experienced fires may also be subjected to low-cycle fatigue caused by earthquakes and other factors, which raises concerns about the low-cycle fatigue performance of materials after exposure to high temperatures. After exposure to high temperatures, a series of complex physical and chemical changes occur inside the concrete, resulting in many small cracks. Under cyclic loading, these microcracks propagate and connect continuously, and the accumulation of microscopic damage eventually leads to macroscopic cracks

and ultimate fatigue failure. Microstructural changes are the inherent cause of macroscopic damage, and studying the relationship between the high-temperature process of materials, low-cycle fatigue damage, and microstructural changes is of great significance for non-destructive or micro-damage detection and fatigue damage evaluation of high-strength concrete structures after a fire. In spite of its excellent fire-resistant performance, the concrete structures after exposure to high temperature must also meet the requirements of the corresponding seismic fortification under the low cycle loading caused by earthquake or other cyclic loadings. It can be seen that some concrete structures of HSC may experience comprehensive working conditions combining high temperature, fatigue and other factors, which will cause fatigue damage to concrete. This damage exists not only at the macro level, but also at the micro level, and there is an objective relationship between macro damage and microstructural change.

In order to scientifically evaluate and repair the fire damaged buildings, its structure must be analyzed. However, it's very difficult to use non-destructive testing methods to determine the temperature history and mechanical properties of building materials, what's more, the limited numbers and uneven temperature field of coring samples will lead an unsatisfactory result, which leads to the hidden dangers of the final assessment conclusion and reinforcement plan. Therefore, it's necessary to put forward the scientific means to study the relationship between high temperature history and microstructure evolution mechanism of HSC and establish the corresponding relationship models.

Nowadays, many research have been carried out to investigate the microstructure of HSC after exposure to high temperature. Muhammad et al. [1] observed microstructural samples after 150, 300, 500, and 800 °C through scanning electron microscopy (SEM) and evaluated the role of poly (1,4-isoprene) particles in the modified system using thermogravimetric analysis (TMA) conducted on hardened cement paste, latex film, and cement-latex blend. Ren et al. [2] studied two high performance concrete materials using the TMA technique between room temperature and 800 °C, and microporosities were observed in the calcium-silicate-hydrate (C-S-H) phase as a result of phase changes during heating. Annerel and Taerwe [3, 4] researched the structural change of HSC after exposure to high temperature by some basic approaches. Liu et al. [5] used differential thermal analysis (DTA), thermogravimetric analysis (TGA), SEM and mercury intrusion porosimetry (MIP) to test the changes of microstructure of high-performance concrete at high temperature. Saridemir et al. [6] examined the crack formation and alterations in the matrix, interface and aggregate of HSCs by X-ray diffraction (XRD), SEM and polarized light microscope (PLM) analyses. XRD, SEM and PLM analyses have shown that increasing target temperature result with decrease in mechanical properties.

Furthermore, some studies focus on fatigue damage of HSC after exposure to high temperature. Oneschkow [7] investigated the fatigue behavior of HSC within a low-cycle-fatigue research project with respect to the influence of maximum stress level, loading frequency and waveform. The influence on numbers of cycles to failure and on the developments of strain and stiffness were systematically analyzed. Kumar et al. [8] and Gao [9] found the maximum longitudinal total strain of the HSC after exposure to high temperature processes under low cyclic uniaxial compressive loading is in accordance with the three-stage development law and established the relationship models between the high temperature process and the fatigue

damage. Yan et al. [10] present an experimental investigation on the compressive behavior of steel fiber-reinforced reactive powder concrete (SRPC) at 20–800 °C, including the failure mode, compressive strength, stress-strain curve and energy absorption capacity. Mathews et al. [11] found through experimental research that high temperature can cause a decrease in the strength of concrete, and the loss of strength increases with the increase of the concrete grade. Yang et al. [12] investigated the changes in the mechanical properties of concrete under compressive and bending fatigue loads, and quantitatively described its fatigue performance through stress-strain curves and fatigue life curves. Chan et al. [13] tested the parameters of residual compressive strength, porosity and pore size distribution of high-performance concrete and normal concrete after exposure to high temperature of 800 degrees Celsius, showing that the strength of HPC degrades faster than normal concrete with increasing exposure temperature, but HPC has higher residual strength. Abdelmelek and Lublóy [14] found that in high-temperature environments, the compressive strength, tensile strength, freeze-thaw resistance, and other properties of mortar containing fly ash decrease. Moreover, as the temperature rises and the duration lengthens, these decreasing trends are intensified. Dehane et al. [15] used advanced imaging techniques to study the effect of saline wastewater on the microstructure of concrete and found that the use of saline wastewater in concrete mixtures leads to the formation of larger and more numerous pores in the concrete structure, which reduces its strength and durability.

Above all, the current research of high strength concrete mainly concentrate on the effect of single factor of high temperature or fatigue damage, while there is a lack of research on the variation of fine microstructure of HSC under comprehensive working conditions, and the relationship between microstructure and mechanical properties of fatigue still absences. So, in this paper, the microstructure of HSC after exposure to high temperature under low cycle compression loading has been studied by means of ultrasonic detection, microhardness test, scanning electron microscope test, mercury intrusion method and XRD. The relationship between microscopic parameters and macroscopic mechanical behaviors is established. On this basis, the dynamic evolution process and damage mechanism of fine microstructure of HSC under the comprehensive conditions of high temperature and fatigue loading are further revealed. The research results can provide references for nondestructive testing, fatigue damage analysis and structural evaluation of concrete structures subjected to fire or other high temperature processes.

2 Materials and experimental methods

2.1 Low cycle compression fatigue test after exposure to high temperature

Standard prism concrete with 100 mm sides were used as test material (the matching ratio is shown in Table 1). The heating rate used in this study was set according to the temperature-time curve of the ISO 834 fire protection standard [16]. When carrying out the heating operation, the top and bottom of the specimen surface is protected by a fireproof barrier material to ensure that the temperature does not develop vertically along the specimen and that the remaining four sides are heated evenly (the specimen is heated as shown in Fig. 1). The design heating temperatures were 200, 400, and 600 °C. Each set of specimens was constantly heated for 1, 2, and 3 h after reaching the specified temperature and then cooled in room temperature [17].

Considering the uneven temperature field, after cooling, the prism specimen was cut into three segments perpendicular to the long side direction, and the cube piece in the middle with even temperature field was taken as the study specimen [18]. The fatigue test was carried out on the electro-hydraulic servo testing machine and the vertical fatigue loads on the test blocks was applied by 500 kN actuator. Cyclic loading waveform was sine wave with frequency of 10 Hz, and the minimum stress level S_{\min} (the ratio of minimum lateral compressive stress σ_{\min} and tensile strength f_t) was 0.10, and the maximum stress level S_{\max} was 0.80, 0.85 and 0.90, respectively. And specimens were loaded to 25%, 50%, 75%, 100% of fatigue life, respectively. The deformation of the test pieces was measured by 50 mm foil resistance rosette strain gauge pasted in the two opposite free surfaces of the specimen [19].

2.2 Microstructure test in fatigue process

The microstructure test was carried out in the experimental center of School of Civil and Transportation Engineering of Beijing University of Civil Engineering and Architecture. Since the requirements of each sub test are different, the four tests are carried out in the order of ultrasonic detection, microhardness test, scanning electron microscope test, mercury intrusion method and XRD test step by step [20–24].

Firstly, the non-metal ultrasonic testing analyzer (NM-4B) whose transmitting frequency is 50 kHz is used for ultrasonic test. Based on diagonal test method, test blocks loaded to 25%, 50%, 75% of the fatigue life were selected, respectively. The diagonal intersection of two unfired sides of the specimens was ultrasonic point and took the distance between two ultrasonic points measured by vernier caliper as distance measurement, as shown in Fig. 2(a). Applied a layer of medical Vaseline evenly on the test points, and pasted the transmitting probe and receiving probe tightly on the concrete measuring points, then gently twisted the probe to discharged the excess air to achieve good acoustic coupling of probe and concrete. Each test point was repeated six times, and the average value was taken as the test result of this point.

Then the microhardness tester (FM-800) was used for the test. The test blocks tested by ultrasonic wave were cut in parallel to the unfired sides and cut into 10 mm thin slices along the centerline, as shown in Fig. 2(b). After grinding and polishing, the specimens were firmly placed on the rigid support of the FM-800 microhardness tester. Carefully adjust the illumination and focus to obtain clear indentation images. Then contact the indenter with the surface of the specimen and increased the test force applied perpendicular to the test surface to the specified value 100 g. The time from loading to all test force applying was 4 s, and then kept the maximum constant test force for 15 s. The microhardness tester should avoid impact and vibration during the whole experiment.

Afterwards, scanning electron microscope (HITACHI S-4300) tests were carried out. First of all, the prepared sample was firstly dusted with an ear wash ball. In order to make the surface of the sample conductive, it was firstly placed in a vacuum coater for evacuation, and after

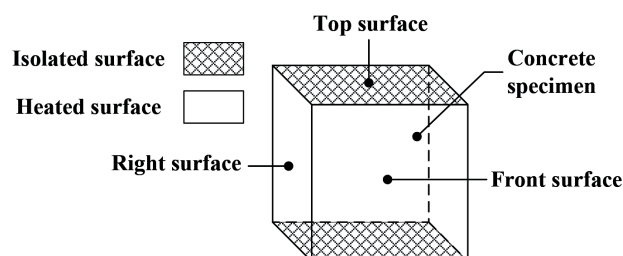


Fig. 1 Schematic diagram of the heated surfaces

Table 1 Mix Properties of HSC

Cement: kg/m ³	Sand: kg/m ³	Gravel: kg/m ³	Water: kg/m ³	Water reducing agent: kg/m ³	Water to binder ratio: kg/m ³
510	720	1040	144	11	0.32

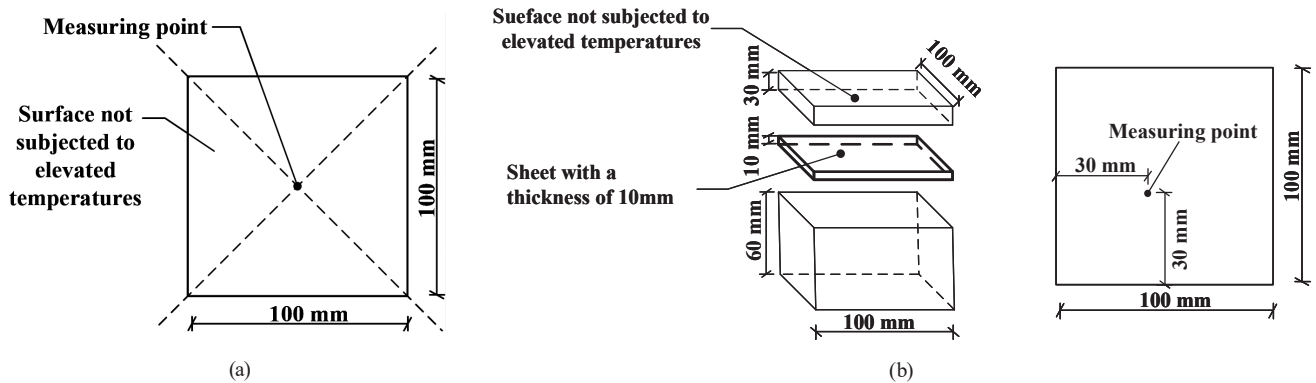


Fig. 2 Test schematic; (a) Schematic diagram of direct-penetration method, (b) Schematic diagram of microhardness test

reaching the vacuum state, a gold film was sprayed on its surface. Then it was glued to the scanning electron microscope carrier plate with a photocell and marked on the carrier plate. Finally, it was sent into the scanning electron microscope sample chamber and fixed. At the same time, the surface morphology was analyzed at different points by adjusting the position and magnification of the objective.

The pore structure of the sample was analyzed by automatic mercury intrusion porosimetry instrument (Autopore IV 9500). Break the specified test block region where microhardness test had been done and loaded to fatigue damage with hammer, and pick out the sample about 10 mm × 10 mm × 10 mm. Before testing, heat the sample in vacuum drying oven under 60 °C for more than 2~3 hours. Then, weigh the empty test tubes and test tubes put into the sample. Next, evacuate the test tubes to vacuum at low pressure, measure the amount of the intruded mercury at high pressure after completion, weigh the test tubes after experiment and record the weight difference. Keep the room temperature below 25 °C and in good ventilation condition. Export data after the experiment.

The samples were tested using an X-ray diffraction (DX-2700B analyzer). Because the samples were inevitably mixed with sand, so after coarse crushing, the remaining samples should as much as possible remove the gravel and coarse sand and so on. Then, the samples were mixed with alcohol and placed in an agate mortar to grind to granule. Carefully collected, and took proper amount onto the load plate, then put in the scanning bin and set the parameters [25].

3 Results and discussion

3.1 Fatigue life

It is generally believed that the fatigue life of concrete is subject to the lognormal distribution [26, 27]. The European Concrete Code uses a formula to predict the fatigue life of concrete, according to which the logarithmic values of the

expected fatigue life of ordinary concrete specimens at room temperature are calculated to be 1.368, 2.052 and 2.736 (corresponding to maximum stress levels of 0.90, 0.85 and 0.80), as shown in equation $\log N = (12 + 16S_{\min} + 8S_{\min}^2)(1 - S_{\max})$. Therefore, the logarithm of the mean value of fatigue life $\lg \bar{N}_f$ under the same stress level is used as the average fatigue life under this condition. At least 3 test blocks are tested for each condition in this test, discrete values are removed, and the average value is taken. The results of the average fatigue life calculation and f_c^T is the compressive strength of HSC specimens after different high temperature processes, whose unit is MPa, as shown in Table 2 [17].

3.2 Results and analysis of microscopic test in fatigue process

3.2.1 Scanning electron microscope tests

Figs. 3 and 4 show SEM images at 30 mm from each of the three adjacent surfaces of the concrete during uniaxial compression fatigue at a stress level of 0.9 at room temperature and 400 °C for 1 h.

Table 2 Test data of fatigue life for HSC after exposure to high temperature

Specimen Number	Average fatigue life ($\lg \bar{N}_f$)		
	$0.9 f_c^T$	$0.85 f_c^T$	$0.8 f_c^T$
P-200-1	3.16	4.53	5.01
P-200-2	2.07	4.34	4.91
P-200-3	2.74	3.60	4.74
P-400-1	2.80	4.83	4.97
P-400-2	2.09	2.82	3.08
P-400-3	2.37	4.65	5.04
P-600-1	3.52	4.74	4.96
P-600-2	3.50	4.80	5.08
P-600-3	1.49	2.32	4.49

Note: P-heating temperature-holding time. Eg.P-200-1 indicates keeping 200 °C for 1 h.

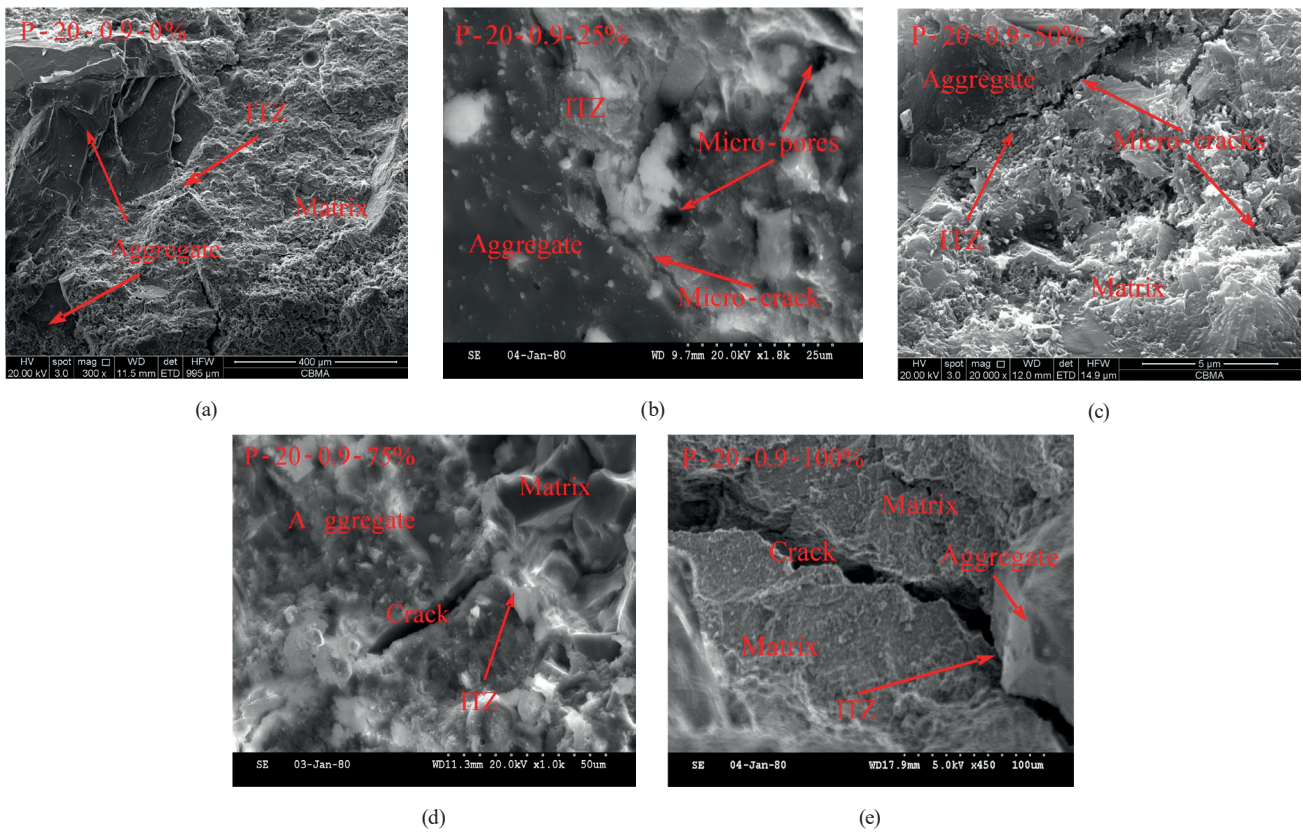


Fig. 3 SEM images during fatigue under the maximum stress level of 0.9 at room temperature; (a) P-20-0.9-0%, (b) P-20-0.9-25%, (c) P-20-0.9-50%, (d) P-20-0.9-75%, (e) P-20-0.9-100%

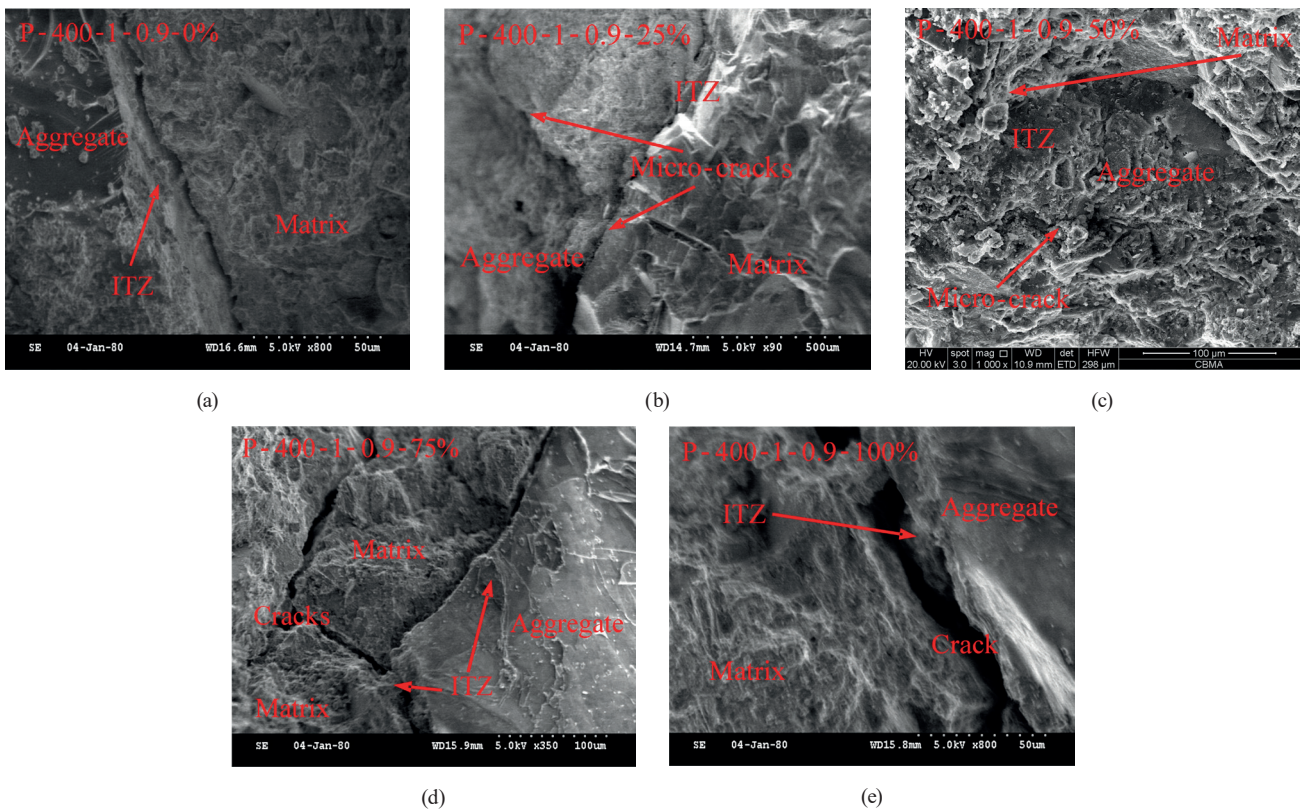


Fig. 4 SEM images during fatigue after exposure to 400 °C and kept for 1 h under the maximum stress level of 0.9; (a) P-400-1-0.9-0%, (b) P-400-1-0.9-25%, (c) P-400-1-0.9-50%, (d) P-400-1-0.9-75%, (e) P-400-1-0.9-100%

Fig. 3(a) shows that the interfacial transition zone (ITZ) between aggregate and cement matrix of HSC is tightly adhered at room temperature, and the cement paste is dense and continuous. The structure is complete, and no obvious defects are found. According to Fig. 4(a), after 1 h with a constantly high temperature of 400 °C, there are obvious defects such as holes and micro-cracks in the transition region of the aggregate and cementite interface before fatigue loading. The cement paste appeared significantly flaky, and the gel surface showed significant crystalline water dissipation after leaving small holes. According to Fig. 3(b) and Fig. 4(b), when the loading reaches 25% of the fatigue life, the porous state in the ITZ of the interface between the aggregate and the cement paste is significantly increased, which generates the hydration products. The cement paste is uncompacted, and the structural looseness is significantly increased. The bond becomes loose, and a large number of micro-cracks is generated. The micro-cracks expand rapidly along the surface of aggregate. As can be seen in Fig. 3(c) and Fig. 4(c), at 50% of the fatigue life, the structure of cement paste becomes significantly flaky and peeled, and the porous state is further aggravated. There are a large number of scattered interconnected micro-cracks developing uniformly within the cement paste, which indicates that the development of micro-cracks is mainly focused in the interior of the cement paste. As can be seen in Fig. 3(d) and Fig. 4(d), when loaded to 75% of the fatigue life, there is severe delamination and misalignment between the aggregate and the cement paste. Cracks are interconnected between the cement paste and the ITZ. Micro-cracks in adjacent coarse aggregates are distributed in parallel or multiple distributions and become larger in width. Some of the cracks extend further which leads to the connection between nearby holes. According to Fig. 3(e) and Fig. 4(e), a large number of deep gaps and voids are generated between the aggregate and the cement paste when loaded to fatigue failure. The gaps penetrate along the edges of the aggregate thus eventually lead to the failure of specimens. In conclusion, fatigue failure first occurs in the ITZ between aggregate and cement paste, which is highly consistent with the macro fatigue failure pattern of high-strength concrete after high temperature.

3.2.2 Ultrasonic detection

The fatigue process of high strength concrete under uniaxial compression after exposure to high temperature is characterized by sonic time.

It can be seen from Fig. 5 that the sonic time varies with the fatigue loading process. When loading to 25% of the fatigue life, the amplitude of sonic time changes greatly, which is about 1.1~1.5 times before loading. When loading from 25% to 75% of the fatigue life, changes of sonic time tend to be gentle. When the holding time and stress level are constant, the higher the heating temperature, the greater the sonic time. What's more, the sonic time at 600 °C is about 4 times as much as it at 200 °C, and the sonic time under loading to 75% of the fatigue life is only about 1.25 times than loading before. Thus, the impact of heating temperature on sonic time is far greater than the fatigue process. Holding time and stress level have less influence on sonic time.

The analysis shows that there are many tiny cracks on the interface and the inner of cement stone before loading. Due to the difference in elastic modulus and strength of aggregate and cement, the deformations of the two materials are not consistent under the fatigue loading. A large amount of microcracks will generate quickly on the interface between aggregate and cement stone at the beginning of the fatigue cycle, resulting in the variation of sonic time. The number of microcracks formed by the cyclic loading is gradually reduced with the increase of the number of fatigue loading, so that the change range of the sonic time at this stage is small. And the microcracks are constantly absorbing the energy, gradually developing, crossing, converging, finally resulting in performance between aggregate and cement stone adhesive cracks and internal microcracks leading to unstable continuous crack instability expansion. Then adjacent microcracks continue to merge to form a macrocrack, test blocks damage [19, 28].

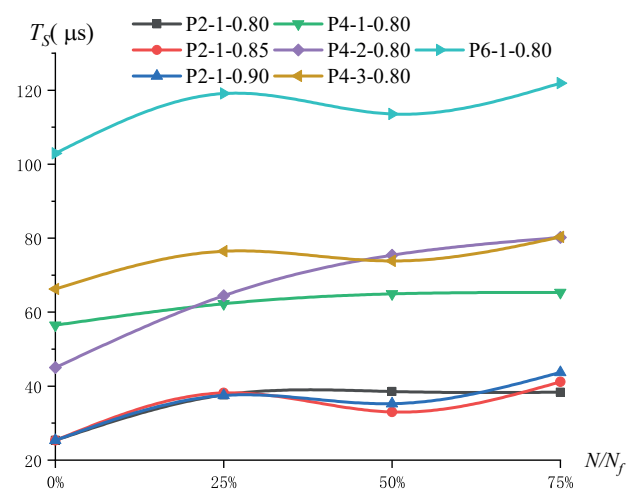


Fig. 5 Relationship between sonic time T_s and relative fatigue cycles N/N_f of HSC after exposure to high temperature

The regression equation of the fatigue strain of HSC after different high temperature process was obtained by nonlinear multivariate regression of the measured sonic time T_s , the number of loading cycles N/N_f and the stress level S_{max} :

$$T_s = a(N/N_f)^3 + b(N/N_f)^2 + c(N/N_f) + dT + et, \quad (1)$$

in which T indicates the heating temperature, t indicates the holding time, N is the number of fatigue loading times, N_f is fatigue life and a, b, c, d, e are coefficients of regression equation.

In order to facilitate the engineering application and analysis, this paper analyzed the relationship between the sonic time T_s and the loading cycles after exposure to different high temperature processes under various stress levels and put forward a unified formula. Holding time was neglected due to its small influence.

When $S_{max} = 0.80, S_{min} = 0.10$:

$$T_s = 1.79(N/N_f)^3 - 15.07(N/N_f)^2 + 41.49(N/N_f) + 0.14T - 0.021t (200^\circ\text{C} < T \leq 600^\circ\text{C}) R^2 = 0.8917. \quad (2)$$

When $S_{max} = 0.85, S_{min} = 0.10$:

$$T_s = 2.08(N/N_f)^3 - 16.17(N/N_f)^2 + 41.43(N/N_f) + 0.14T - 0.011t (200^\circ\text{C} < T \leq 600^\circ\text{C}) R^2 = 0.9915. \quad (3)$$

When $S_{max} = 0.90, S_{min} = 0.10$:

$$T_s = 0.99(N/N_f)^3 - 10.36(N/N_f)^2 + 35.22(N/N_f) + 0.14T - 0.016t (200^\circ\text{C} < T \leq 600^\circ\text{C}) R^2 = 0.9789. \quad (4)$$

Furthermore, the relationships between the sonic time T_s of HSC and the strain $\varepsilon_{T,m}$ in fatigue direction under different stress levels and temperature processes were obtained [26]:

When $S_{max} = 0.80, S_{min} = 0.10$:

$$T_s = \left\{ \begin{aligned} &0.0207\varepsilon_{T,m} - 10.7013(N/N_f)^3 + 5.1946(N/N_f)^2 \\ &+ 33.6360(N/N_f) - 3.9446t - 58.2621 \end{aligned} \right\} \quad (5)$$

($200^\circ\text{C} < T \leq 600^\circ\text{C}$) $R^2 = 0.8346$.

When $S_{max} = 0.85, S_{min} = 0.10$:

$$T_s = \left\{ \begin{aligned} &0.0226\varepsilon_{T,m} - 26.4236(N/N_f)^3 + 15.0759(N/N_f)^2 \\ &+ 11.6153(N/N_f) - 10.5313t - 43.1240 \end{aligned} \right\} \quad (6)$$

($200^\circ\text{C} < T \leq 600^\circ\text{C}$) $R^2 = 0.9347$.

When $S_{max} = 0.90, S_{min} = 0.10$:

$$T_s = \left\{ \begin{aligned} &0.0152\varepsilon_{T,m} - 23.5225(N/N_f)^3 + 14.1453(N/N_f)^2 \\ &+ 19.5123(N/N_f) - 2.8524t - 40.9018 \end{aligned} \right\} \quad (7)$$

($200^\circ\text{C} < T \leq 600^\circ\text{C}$) $R^2 = 0.8861$.

In order to facilitate the fatigue damage analysis and structural evaluation of HSC structures subjected to fire or other high temperature history by means of non-destructive testing, a fitting of the sonic time T_s of HSC and fatigue strain $\varepsilon_{T,m}$ of HSC under different temperature conditions was proposed:

$$\varepsilon_{T,m} = 1030.70T_s^{0.422} \quad R^2 = 0.9166. \quad (8)$$

3.2.3 Microhardness test

It can be seen from Fig. 6 that the microhardness (HV) of concrete under the increasing fatigue loading reduced in three phrases. Take the concrete at 400°C for example, the HV under the loading before fatigue to 25% of fatigue life changed rapidly and reduced by about 20% while its variation tended to moderate under the loading from 25% to 75% of the fatigue life and reduced roughly by 10%. Comparing with the different holding time and stress

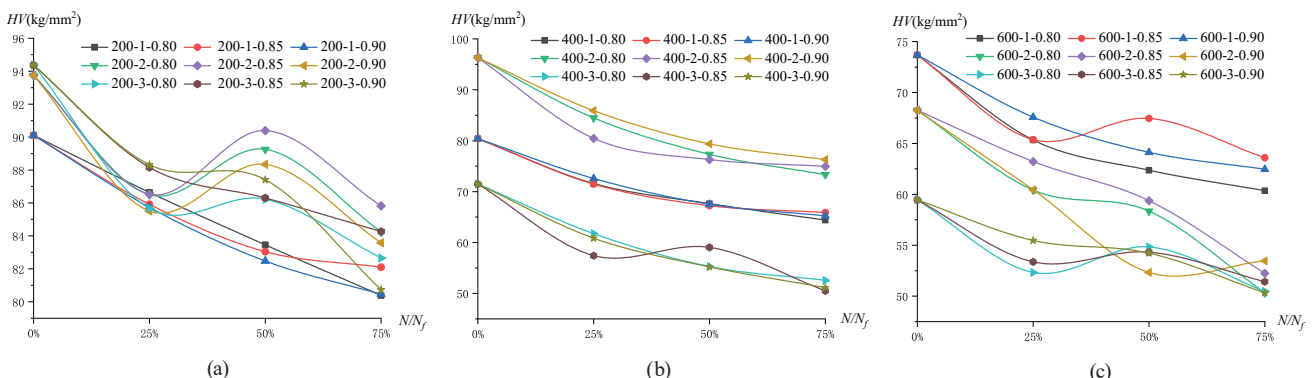


Fig. 6 Relationship between micro-hardness and relative fatigue cycles of HSC after high temperature; (a) 200°C , (b) 400°C , (c) 600°C

level, the different heating temperature had a greater influence on HV . When the heating temperature is the same and the constant temperature is different, the HV decreases with the increase of the holding time. Therefore, the HV in the interfacial transition zone (ITZ) decreases continuously from fast to slow with the increase of fatigue loading times. This trend is consistent with the changes pattern of sonic time, and both are well supported. The test results are shown in Fig. 6.

The regression equation of the fatigue strain of HSC after different high temperature process was obtained by nonlinear multivariate regression of the HV , the number of loading cycles N/N_f and the stress level:

$$HV = j(N/N_f)^3 + k(N/N_f)^2 + l(N/N_f) + mT + nt, \quad (9)$$

in which T indicates the heating temperature, t indicates the holding time, N is the number of fatigue loading times, N_f is fatigue life, and j, k, l, m, n are coefficients of regression equation.

In order to facilitate the engineering application and analysis, this paper analyzed the relationship between HV , fatigue strain and the loading cycles after different high temperature processes under various stress levels and put forward the relationship between HV and fatigue strain $\varepsilon_{T,m}$.

When $S_{\max} = 0.80, S_{\min} = 0.10$:

$$HV = \left\{ \begin{array}{l} -0.0081\varepsilon_{T,m} + 4.8345(N/N_f)^3 - 7.8432(N/N_f)^2 \\ -1.2570(N/N_f) + 1.5271t - 120.5222 \end{array} \right\}$$

(200°C < T ≤ 600°C) $R^2 = 0.8614$. (10)

When $S_{\max} = 0.85, S_{\min} = 0.10$:

$$HV = \left\{ \begin{array}{l} -0.0078\varepsilon_{T,m} + 9.8536(N/N_f)^3 - 10.8010(N/N_f)^2 \\ +7.0905(N/N_f) + 3.6409t + 111.2199 \end{array} \right\}$$

(200°C < T ≤ 600°C) $R^2 = 0.9442$. (11)

When $S_{\max} = 0.90, S_{\min} = 0.10$:

$$HV = \left\{ \begin{array}{l} -0.0056\varepsilon_{T,m} + 9.0798(N/N_f)^3 - 9.2618(N/N_f)^2 \\ +1.6385(N/N_f) + 1.0563t - 113.3112 \end{array} \right\}$$

(200°C < T ≤ 600°C) $R^2 = 0.8712$. (12)

In order to facilitate the fatigue damage analysis and structural evaluation of HSC structures subjected to fire or other high temperature history by means of non-destructive

testing, a fitting of HV of HSC and fatigue strain $\varepsilon_{T,m}$ of HSC under different temperature conditions was proposed:

$$HV = -0.0123\varepsilon_{T,m} + 153.0590 \quad R^2 = 0.8209. \quad (13)$$

3.2.4 Mercury intrusion method

The peak aperture in the aperture distribution map is the most probable aperture [29], as shown in Fig. 7. In the case of 400 °C, the most probable aperture increased evidently by about 20% under the loading before fatigue to 25% of the fatigue life, increased small under the loading from the 25% of the fatigue life to 50% and 50% to 75% by about 6% and 6.3%, respectively. The amplification is 12% under the loading from 75% of the fatigue life to fatigue damage. Thus, the most probable aperture shows the three-stage change trend of the "fast-slow-fast" process with the fatigue loading process, which confirms the three-stage rule of the macroscopic mechanical behavior from the microscopic level and is consistent with the variation trend of sonic time and microhardness well.

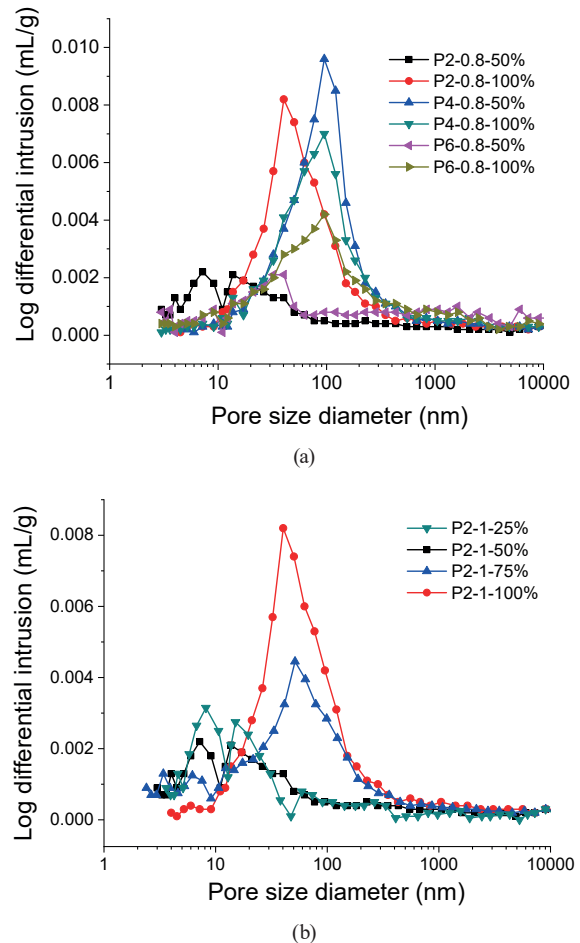


Fig. 7 Pore size distribution, (a) Different temperatures, (b) Different levels of fatigue

Table 3 The amount of mercury injected in different pore sizes

No.	Specimen No.	The most probable aperture size	Accumulate mercury volume	<50 nm/%	50~200 nm/%	>200 nm/%	Peak width
1	P2-1	50.3	0.0580	49.8	30.5	19.7	11~151.1
	P2-1-0.9-25%	62.5	0.0618	42.2	37.7	20.1	11~183.2
	P2-1-0.9-50%	68.5	0.0610	36.9	40.3	22.8	12.2~227.1
	P2-1-0.9-75%	73.1	0.0643	30.2	44.5	25.3	12.2~227.1
	P2-1-0.9-100%	85.4	0.0678	23.7	48.8	27.5	17.1~283.5
2	P4-1	77.1	0.0616	31	40.4	28.6	13.7~283
	P4-1-0.85-25%	88.5	0.0653	27	49.9	23.1	13.7~283
	P4-1-0.85-50%	95.4	0.0661	21.8	51.6	26.6	21.1~350.5
	P4-1-0.85-75%	87.3	0.0685	19.3	50.5	30.2	13.7~283
	P4-1-0.85-100%	98.6	0.0718	21	54.2	24.8	21.1~434
3	P4-3	95.4	0.0654	22.3	44.2	33.5	17.1~434.8
	P4-3-0.85-25%	108.7	0.0708	17.7	48.7	33.6	21.1~554.0
	P4-3-0.85-50%	101.3	0.0735	18	47.2	34.8	17.1~554.0
	P4-3-0.85-75%	113.6	0.0756	18.3	43.9	37.8	21.1~677.9
	P4-3-0.85-100%	120.8	0.0789	13.1	48.6	38.3	26.3~836.6
4	P6-1	77.1	0.0727	22.6	42.6	34.8	17.1~283.9
	P6-1-0.85-25%	95.6	0.0749	22.8	46.4	30.8	21.1~350.1
	P6-1-0.85-50%	95.6	0.0759	21	45.1	33.9	21.1~350.1
	P6-1-0.85-75%	85.1	0.0751	18.1	47.8	34.1	17.1~434.8
	P6-1-0.85-100%	102.1	0.0788	15.4	49.4	35.2	21.1~434.8

Note: pore size distribution expressed as a percentage

It can be seen from Fig. 7 and Table 3 that the increase of the number of fatigue loading cycles enlarges the most probable aperture in the transition zone of aggregate-cement stone interface of HSC after exposure to high temperature evidently. The pores with the size of more than 50 nm are harmful holes and more hazardous holes, while those with the size of less than 50 nm are less harmful holes and harmless holes [29]. When the HSC test block is loaded to 70% of the fatigue life, the number of harmful holes and increased obviously, and the number of less harmful holes and harmless holes reduced to a certain extent. The reason shows that the number of harmful holes and more hazardous holes in the transition zone of the aggregate-cement interface before fatigue loading are relatively small. At the beginning of the fatigue cycle loading, the pores in the transition zone absorb energy quickly expanding the edge of the holes, so that the pore size increases and part of the less harmful holes and harmless holes develop into. Then the number of less harmful holes and harmless holes decreases and harmful holes and more hazardous holes increases, which ultimately lead to test blocks damage.

3.2.5 XRD test

Fig. 8 shows the XRD pattern with details of the crystalline phases present in the samples, which were loading under 0.9 of stress level after heating at 200 °C for 1 h [30]. XRD data were obtained by using a X-ray diffractometer with the following testing parameters: 30 KV, 40 mA, and Cu K α

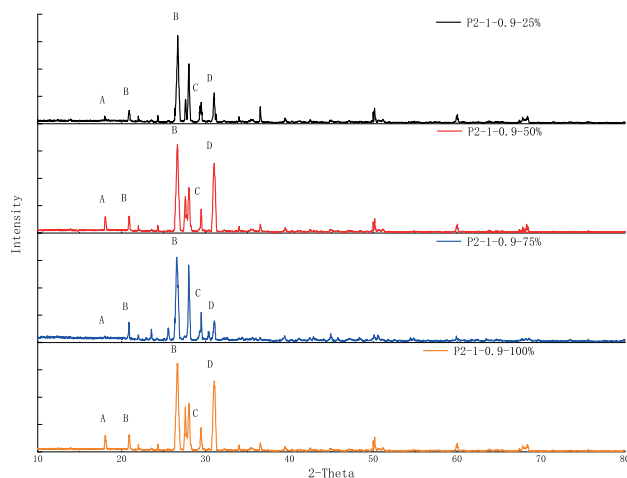


Fig. 8 The XRD pattern; the peaks are identified as follows: A = calcium hydroxide or Ca(OH)₂, B = quartz or SiO₂, C = calcium carbonate or CaCO₃, and D = dolomite or MgCO₃·CaCO₃

radiation. The XRD patterns were obtained by a scanning rate of one degree per minute from 10 to 80 degrees (2θ) and steps of 0.02 degrees (2θ).

A single letter or set of letters was assigned to each phase to facilitate easier representation. The major components of samples are quartz (SiO_2) and dolomite ($\text{MgCO}_3 \cdot \text{CaCO}_3$). The presence of a broad elevation hump from 20° to 40° , indicates the presence of amorphous silicates, which are difficult to characterize [31]. Compared with the samples before fatigue loading [18], there was no obvious change, indicating that the basic reaction of cement mineral phase before fatigue loading was completed. There were almost no characteristic peaks of tricalcium silicate, dicalcium silicate, tricalcium aluminate and tetracalcium aluminate which indicated that the contents were very few and almost completely reacted. The characteristic peak of hydrated product calcium hydroxide was very low, indicating that there was certain content of calcium hydroxide; the characteristic peak of hydrated product ettringite barely showed almost no ettringite exists; the content of quartz stone was high, mainly from the aggregate. As shown in Fig. 8, the peak value of the hydrated product calcium hydroxide and ettringite was almost invisible when loading to the 25%, 50%, 75% of the fatigue life and even to fatigue damage, indicating that the content of calcium hydroxide and ettringite was almost none, the content of calcium carbonate remained unchanged, and the content of quartz content was high.

In summary, the content of cement hydration products of HSC in the fatigue process after exposure to high temperature kept consistent with it before fatigue and no new minerals formed, which showed that the fatigue process had no obvious effect on the content of HSC. This conclusion is consistent with the results of literature [32].

4 Discussions

By testing and analyzing the microscopic parameters such as sonic time, microhardness, the most probable maximum aperture and cumulative pumping, the three-stage rule of macroscopic mechanical behavior was confirmed from the microcosmic level. And the variation trend of each microscopic parameter was consistent and well supported by each other. From the Eqs. (8) to (12) we can see that the T_s and HV are linearly related to the longitudinal fatigue strain $\varepsilon_{T,m}$, respectively, further illustrating the objective relationship between the microstructure change and the macroscopic damage, confirming the consistency of three-stage change rule.

The rangeability of sonic time, microhardness, the most probable maximum aperture and cumulative pumping shows the trend of fast-slow-fast, an obvious three-stage change rule, indicating that the damage development of its inner micro cracks can be divided into three stages, which is consistent with the three-stage variation of the low cycle compressive fatigue longitudinal total strain of HSC after exposure to high temperature [26]. The first stage is fatigue before loading to loading to 25% of the fatigue life when microcracks develop rapidly. At this stage, the pores in the transition zone of the aggregate-cement stone interface absorb energy fast, the pore size and the cumulative amount of mercury increase rapidly, resulting in the transition zone loose and porous. Then sonic time increases significantly, microhardness decreases, microcracks form and extend substantially along the boundaries of the aggregate. The second stage is under the fatigue loading from 25% of the fatigue life to 75% of the fatigue life, that is, the linear development stage of the microcracks. The damage at this stage is mainly caused by the formation of new microcracks in cement mortar and the stable expansion of the original microcracks. With the increase of the number of fatigue loading times, the amplitude of variation of sonic time, microhardness, the most probable maximum aperture and cumulative pumping tend to be gentle. The inner microcracks increase steady, total longitudinal fatigue strain grows cumulatively linearly, and the growth rate is relatively stable. The third stage is under the loading from 75% of fatigue life to fatigue failure. This phase aperture and cumulative pumping change rapidly. The microcracks expand significantly, interconnect with each other and penetrate the cohesive cracks on the interface of aggregate-cement stone leading to the formation of macrocracks with certain size. Then these cracks intersect with other cracks under the fatigue cycle loading to form larger cracks, which cause the total longitudinal fatigue strain to increase suddenly and damage the specimens eventually.

By performing a nonlinear multivariate regression on the measured ultrasonic velocity, microhardness, and most significant pore size with loading cycle numbers, a relationship model between the microstructure and fatigue process of high-strength concrete after different high-temperature histories under various stress levels was obtained. This model can provide reference for engineering applications and analysis.

5 Conclusions

Based on analysis of experimental results from the development of microstructure, the following conclusions can be drawn below.

1. The variation range of microscopic parameters show an overall trend of fast-slow-fast with the fatigue loading process. The number of harmful holes and more hazardous holes increases significantly, the number of less harmful holes and harmless holes reduces to a certain extent, and the sonic time and microhardness are linearly related to the total longitudinal fatigue strain. By establishing the relationship model between the microscopic parameters and the total longitudinal fatigue strain, the three-stage rule of the macroscopic mechanical behavior is confirmed from the microcosmic level.

2. The fatigue loading process has no obvious effect on the content of each phase in the high strength concrete, but has a great influence on the pore structure, which is far less important than the influence of heating temperature. And the pore structure of high strength concrete in fatigue process after exposure to high temperature has no obvious changes with the variation of holding time and stress level.

3. The variation rules of the measured parameters through five microscopic test methods are consistent and well supported by each other. Also, these rules definite the

three-stage damage development of the inner microcracks of high strength concrete in the fatigue loading process and further reveal the dynamic evolution process and the fatigue damage mechanism of the internal fine microstructure of the high strength concrete under the comprehensive conditions of high temperature and fatigue loading.

The micro-scale fatigue damage accumulation model and the comprehensive fatigue damage accumulation model established in this article are only based on C60 concrete, and the heating temperature is only tested at 200 °C, 400 °C and 600 °C. Further improvement is needed in future research for other strength concretes or more complex working conditions.

Acknowledgements

The present work was supported by the National Natural Science Foundation of China (No. 51378045), the Open Research Fund Program of Engineering Structure and New Materials of Beijing University Engineering Research Center (Beijing University of Civil Engineering and Architecture), Beijing Advanced Innovation Center for Future Urban Design, and the Beijing Collaborative Innovation Center of Energy Conservation and Emissions Reduction Technology. The authors gratefully acknowledge the mentioned support.

References

- [1] Muhammad, B., Ismail, M., Haron, Z., Yussuf, A. A. "Elastomeric effect of natural rubber latex on compressive strength of concrete at high temperatures", *Journal of Materials in Civil Engineering*, 23(12), pp. 1697–1702, 2011.
[https://doi.org/10.1061/\(ASCE\)MT.1943-5533.0000338](https://doi.org/10.1061/(ASCE)MT.1943-5533.0000338)
- [2] Ren, F., Wang, J. J.-A., DiPaolo, B. P. "Thermal expansion study and microstructural characterization of high-performance concretes", *Journal of Materials in Civil Engineering*, 25(10), pp. 1574–1578, 2013.
[https://doi.org/10.1061/\(ASCE\)MT.1943-5533.0000693](https://doi.org/10.1061/(ASCE)MT.1943-5533.0000693)
- [3] Annerel, E., Taerwe, L. "Basic approach for the diagnosis of concrete after fire exposure", *Journal of Structural Fire Engineering*, 1(3), pp. 135–144, 2010.
<https://doi.org/10.1260/2040-2317.1.3.135>
- [4] Annerel, E., Taerwe, L. "Diagnosis of the state of concrete structures after fire", In: Walraven, J. C., Stoelhorst, D. (eds.) *Tailor Made Concrete Structures*, Taylor & Francis Group, 2008, pp. 257–262. ISBN: 978-0-415-47535-8
<https://doi.org/10.1201/9781439828410.ch46>
- [5] Liu, X., Yuan, Y., Ye, G., Geert, D. S. "Study on pore structure evolution of high performance concrete with elevated temperatures", *Journal of Tongji University (Natural Science)*, 36(11), pp. 1473–1478, 2008. (in Chinese)
<https://doi.org/10.3321/j.issn:0253-374X.2008.11.004>
- [6] Saridemir, M., Severcan, M. H., Ciflikli, M., Celikten, S., Ozcan, F., Atis, C. D. "The influence of elevated temperature on strength and microstructure of high strength concrete containing ground pumice and metakaolin", *Construction and Building Materials*, 124, pp. 244–257, 2016.
<https://doi.org/10.1016/j.conbuildmat.2016.07.109>
- [7] Oneschkow, N. "Fatigue behaviour of high-strength concrete with respect to strain and stiffness", *International Journal of Fatigue*, 87, pp. 38–49, 2016.
<https://doi.org/10.1016/j.ijfatigue.2016.01.008>
- [8] Kumar, R., Singh, S., Singh, L. P. "Studies on enhanced thermally stable high strength concrete incorporating silica nanoparticles", *Construction and Building Materials*, 153, pp. 506–513, 2017.
<https://doi.org/10.1016/j.conbuildmat.2017.07.057>
- [9] Gao, H. "Research on the compressive fatigue properties of HSC after different high temperature process", MSc Thesis, Beijing University of Civil Engineering and Architecture, 2017. (in Chinese) [online] Available at: <https://kns.cnki.net/KCMS/detail/detail.aspx?dbname=CMFD201801&filename=1017169855.nh>
- [10] Yan, K., Xu, C., Zhang, X. "Compressive Behaviour of Steel Fiber-Reinforced Reactive Powder Concrete at Elevated Temperatures", *Science of Advanced Materials*, 8(7), pp. 1454–1463, 2016.
<https://doi.org/10.1166/sam.2016.2758>

- [11] Mathews, M. E., Kiran, T., Naidu, V. C. H., Jeyakumar, G., Anand, N. "Effect of high-temperature on the mechanical and durability behaviour of concrete", *Materials Today: Proceedings*, 42(2), pp. 718–725, 2021.
<https://doi.org/10.1016/j.matpr.2020.11.153>
- [12] Yang, Z., Li, H., Wen, J., Huang, F., Wang, Z., Yi, Z., Xie, Y., Dong, H. "The microstructure evolution of ballastless track high-strength concrete exposed to compressive and flexural fatigue loads", *International Journal of Fatigue*, 166, 107247, 2023.
<https://doi.org/10.1016/j.ijfatigue.2022.107247>
- [13] Chan, Y. N., Luo, X., Sun, W. "Compressive strength and pore structure of high-performance concrete after exposure to high temperature up to 800°C", *Cement and Concrete Research*, 30(2), pp. 247–251, 2000.
[https://doi.org/10.1016/S0008-8846\(99\)00240-9](https://doi.org/10.1016/S0008-8846(99)00240-9)
- [14] Abdelmelek, N., Lublóy, É. "Effects of Elevated Temperatures on the Properties of High Strength Cement Paste Containing Silica Fume", *Periodica Polytechnica Civil Engineering*, 66(1), pp. 127–137, 2022.
<https://doi.org/10.3311/PPci.17549>
- [15] Dehane, S., Kriker, A., Salhi, A. "Influence of Saline-treated Wastewater on Properties of Concrete: An Experimental Study", *Periodica Polytechnica Civil Engineering*, 2023.
<https://doi.org/10.3311/PPci.21841>
- [16] ISO "ISO-834 Fire-resistance tests - Elements of building construction", International Organization for Standardization, Geneva, Switzerland, 1975.
- [17] Zhao, D., Gao, H., Jia, P., Wen, H., Yang, J. "Performance degradation of high strength concrete (HSC) after different-high-temperature history", *Journal of Vibration and Shock*, 37(04), pp. 240–248, 2018. (in Chinese)
[10.13465/j.cnki.jvs.2018.4.036](https://doi.org/10.13465/j.cnki.jvs.2018.4.036)
- [18] Zhao, D., Liu, M. "Experimental study on residual strength and nondestructive testing of high strength concrete after high temperature", *Journal of Building Structures*, 36(2), pp. 365–372, 2015. (in Chinese)
<https://doi.org/10.14006/j.jzjgxb.2015.S2.053>
- [19] Zhao, D., Gao, H., Liu, H., Jia, P., Yang, J. "Fatigue properties of plain concrete under triaxial tension-compression-compression cyclic loading", *Shock and Vibration*, 2017, 9351820, 2017.
<https://doi.org/10.1155/2017/9351820>
- [20] Mikami, C., Wu, H.-C., Elarbi, A. "Effect of hot temperature on pull-off strength of FRP bonded concrete", *Construction and Building Materials*, 91, pp. 180–186, 2015.
<https://doi.org/10.1016/j.conbuildmat.2015.05.013>
- [21] Li, L., Xie, W. "Performance of 100 MPa High Strength Concrete", *Advanced Science Letters*, 4(8-9), pp. 2623–2630, 2011.
<https://doi.org/10.1166/asl.2011.1725>
- [22] Li, Q., Gao, X., Xu, S., Peng, Y., Fu, Y. "Microstructure and mechanical properties of high-toughness fiber-reinforced cementitious composites after exposure to elevated temperatures", *Journal of Materials in Civil Engineering*, 28(11), 04016132, 2016.
[https://doi.org/10.1061/\(ASCE\)MT.1943-5533.0001647](https://doi.org/10.1061/(ASCE)MT.1943-5533.0001647)
- [23] Henry, M., Darma, I. S., Sugiyama, T. "Analysis of the effect of heating and re-curing on the microstructure of high-strength concrete using X-ray CT", *Construction and Building Materials*, 67, pp. 37–46, 2014.
<https://doi.org/10.1016/j.conbuildmat.2013.11.007>
- [24] M'Jahad, S., Davy, C. A., Bourbon, X., Skoczylas, F. "Water retention and gas migration of two high-performance concretes after damage", *Journal of Materials in Civil Engineering*, 27(2), A4014008, 2015.
[https://doi.org/10.1061/\(ASCE\)MT.1943-5533.0001028](https://doi.org/10.1061/(ASCE)MT.1943-5533.0001028)
- [25] You, Z. "Research on performance damage of reinforced concrete beam after fire", MSc Thesis, Beijing University of Civil Engineering and Architecture, 2013. (in Chinese) [online] Available at: <https://kns.cnki.net/KCMS/detail/detail.aspx?dbname=CMFD201302&filename=1013281826.nh>
- [26] Cheong, H. K., Zeng, H. "Stress-strain relationship for concrete confined by lateral steel reinforcement", *ACI Materials Journal*, 99(3), pp. 250–255, 2002.
<http://doi.org/10.14359/11970>
- [27] McCall, J. T. "Probability of fatigue failure of plain concrete", *ACI Journal Proceedings*, 55(2), pp. 233–244, 1958.
<http://doi.org/10.14359/11351>
- [28] Wu, Z., Lian, H. "High performance concrete", China Railway Publishing House, 1999. ISBN 7-113-03458-6 (in Chinese)
- [29] Zhao, D. "Study on failure criterion of plain concrete under multiaxial fatigue loading", PhD Thesis, Dalian University of Technology, 2001. [online] Available at: <https://kns.cnki.net/KCMS/detail/detail.aspx?dbname=CDFD9908&filename=2003110421.nh>
- [30] Lian, H., Dong, L., Cheng, E. "Building materials phase research foundation", Tsinghua University Press, 1996. ISBN 7-302-02071-X (in Chinese)
- [31] Nagalia, G., Park, Y., Abolmaali, A., Aswath, P. "Compressive strength and microstructural properties of fly ash-based geopolymer concrete", *Journal of Materials in Civil Engineering*, 28(12), 04016144, 2016.
[https://doi.org/10.1061/\(ASCE\)MT.1943-5533.0001656](https://doi.org/10.1061/(ASCE)MT.1943-5533.0001656)
- [32] Li, X., Bao, Y., Xue, N., Chen, G. "Bond strength of steel bars embedded in high-performance fiber-reinforced cementitious composite before and after exposure to elevated temperatures", *Fire Safety Journal*, 92, pp. 98–106, 2017.
<https://doi.org/10.1016/j.firesaf.2017.06.006>